Optics Letters

Experimental demonstration of laser damage caused by interface coupling effects of substrate surface and coating layers

Yingjie Chai,[1,2] Meiping Zhu,[1,*] Kui Yi,[1] Weili Zhang,[1] Hu Wang,[1,2] Zhou Fang,[1,2] Zhengyuan Bai,[1,2] Yun Cui,[1] and Jianda Shao[1]

[1]Key Laboratory of Materials for High Power Laser, Shanghai Institute of Optics and Fine Mechanics, Chinese Academy of Sciences, Shanghai 201800, China
[2]University of Chinese Academy of Sciences, Beijing 100049, China
*Corresponding author: bree@siom.ac.an

Received 27 April 2015; revised 7 July 2015; accepted 8 July 2015; posted 9 July 2015 (Doc. ID 239785); published 5 August 2015

The laser damage resistance of the coatings for high-power laser systems depends greatly on the surface quality of the substrate. In our work, experimental approaches were employed to understand the interface coupling effect of the substrate surface and coatings on the laser resistance of the coatings. A 1064 nm anti-reflection (AR) coating was deposited by an e-beam coater onto fused silica with and without micro-scale pits (structural defects). The micro-scale pits were precisely fabricated by femtosecond laser processing to prevent the emergence of subsurface cracks. Different deposition temperatures were characterized in order to verify the intensity of the interface coupling effect of the substrate and coating layers. Our experimental results indicate that impurities that are introduced in the finishing process, shifted to the substrate surface, and aggregated during the heating process, play a much more crucial role than structural defects (length: ~7 μm; width: ~3 μm; depth: ~0.8 μm) in the laser-induced damage process. By effectively reducing the intensity of the interface coupling effect, the e-beam AR coatings, whose laser-induced damage resistance was closed to the bare substrate, was prepared.

OCIS codes: (140.3330) Laser damage; (310.6870) Thin films, other properties; (140.3440) Laser-induced breakdown; (220.4000) Microstructure fabrication.

http://dx.doi.org/10.1364/OL.40.003731

Optical coatings prepared by an e-beam deposition process and a sol-gel method are widely used in high-power laser systems. The laser-induced damage of the optical coating is a limiting factor in the development of high-power laser systems [1]. Recent studies have showed that scratches [2,3] and impurities [4,5] are two major defects in substrate surface factors that influence the laser-induced damage threshold (LIDT) of optical coatings. Substrate scratches have been shown to have negative effects on the laser-induced damage performance of high-reflection (HR) coatings. The correlations between the LIDT and the physical properties of substrate scratches have been elucidated through experiments, and laser-induced damage occurs in the regions of the coatings where the substrate scratches reside [2,3]. However, the impact of substrate structural defects on anti-reflection (AR) coatings is not well defined, and the common physical structural defects in the substrate contain an extensive amount of absorption impurities, the effects of which cannot be easily separated [6]. The LIDT of the sol-gel coating is on par with uncoated, fused silica substrates [7], but the laser damage resistance of the e-beam AR coating on fused silica substrates is lower than the substrate surface itself. This phenomenon indicates the existence of an interface coupling effect between the substrate surface and the coating layers. In Yang and co-workers' work, a high density point and linear bulges were observed after hours of heating [8,9], and by using Time-of-Flight Secondary Ion Mass Spectrometry, the metallic distribution changed near the surface (at a depth of ~45 nm from the surface). The influence of high-absorption defects at the film-substrate interface under ultraviolet laser (3ω) irradiation showed that the defect features in the multilayer coatings originating from the substrate surface play important roles in limiting the LIDT [3].

In this study, we adopted a three-step systematic approach for our experiment. First, the LIDTs of the 1064 nm AR coatings deposited on fused silica substrates with and without micro-scale pits (fs-pits) were characterized and compared. The pits were precisely fabricated by a femtosecond laser pulse to prevent subsurface cracks and adventive impurities which might be introduced during the chemicomechanical polishing process [10–12]. Second, SiO_2 monolayers were prepared by either e-beam deposition or a sol-gel process, and evaluated based on their laser damage performance. Third, different coating temperatures were applied to verify the hypothesis that the

heating process influences the intensity of the interface coupling effects. Simultaneously, in order to determine the intensity of the interface coupling effect, a substrate with 200 nm hydrofluoric acid (HF) etching was also applied [5].

All experiments were conducted on the same group of fused silica with dimensions of 50 mm in diameter and 5 mm in thickness. The cleaning, fabricating, and coating processes were operated in a Class 1000 cleanroom (FED-STD-209E). All substrates were supersonic cleaned (SSC). The fs-pits were precisely fabricated using a femtosecond bench [13]. A Ti:sapphire laser system (Legend USP, Coherent Inc.) with an operating wavelength of 800 nm, a pulse width of 40 fs, and a repetition rate of 1 kHz was used. The laser power was set at 10 mW before focusing on the sample surface with a 20× OLYMPUS microscope objective. The dimension of the fabricated defects were as follows: length, ∼7 μm; width, ∼3 μm; and depth, ∼0.8 μm [3].

All e-beam AR coatings were deposited on the substrates by the e-beam process in a Leybold coater. A vacuum system containing a cryo-pump and a Meissner trap was engaged to reach the starting pressure of 2.7×10^{-4} Pa. The ambient pressure for both HfO_2 and SiO_2 was about 2×10^{-2} Pa. The SiO_2 was deposited at a rate of about 0.6 nm/s, while the HfO_2 was evaporated at a lower rate of about 0.3 nm/s. The AR coating was designed by the commercial software essential Macleod. The HfO_2 and SiO_2 were chosen as high (H) and low (L) refractive index materials respectively; both H and L had a quarter-wave optical thickness at the reference wavelength of 1064 nm (H: 138 nm, L: 183 nm). AR coatings with a layer structure S/2L0.5H1.25L/A were deposited on the substrates with and without fs-pits (shown in Table 1). For LIDT comparisons, a sol-gel S/L/A layer structure was prepared on the fused silica, the same group of substrates of EB-1, by a dip-coating process with a 5–10 cm/ min withdrawal rate. Then, four groups of AR coatings with a structure of S/2L0.5H1.25L/A were deposited by the e-beam process on the fused silica substrate (as shown in Table 1) in the above-mentioned e-beam coater. Samples A1 and A2 were coated at a higher temperature (200°C) to promote the shifting of impurities. HF etching can remove the fused silica surface chemically, where the "invisible" and low-threshold absorbent defects reside [5]. Samples A2 and B2 were chemically etched in a buffered hydrofluoric (1% HF and 15% NH_4F solution) acid to remove ∼200 nm of the surface material before SSC to improve the substrate surface quality. The reflections of all the e-beam samples were measured by a spectrometer (Lambda 1050 UV/VIS/NIR, Perkin-Elmer). All of the reflectances of the e-beam samples were lower than 0.5% at 1064 nm.

The LIDT testing was adapted from ISO standard 11254 for one-on-one irradiation. Mainly due to the uncertainty of the nonuniformity among the samples (3%), the measurement of laser spot area (5%), and the fluctuation of laser energy (5%), the relative error of damage probability amounts to ±15% [14–16]. A Nd:YAG laser produced a 10–12 ns pulse operated at the 1064 nm wavelength in single longitudinal mode with up to a 5 Hz repetition rate. The e^{-2} spot diameters along the x and y-axes were 397 μm (see in Ref. [17]). The 1064 nm laser was focused on the coating (front) surface of the sample. A visible He–Ne laser was used as the illumination source. The damage was judged by making a comparison of the test area before and after laser irradiation. The X–Y sample stages were adjusted, and we tried to make every shot land in a pit [3]. To prevent the neighboring damage sites from having any impact on each other, the site spacing was 1.5 mm, which was about three times larger than that of the laser spot diameter. Twenty sites for each energy density were tested, and the morphologies of damaged sites were recorded. The LIDT was defined as the energy density of the incident pulse when the damage probability was 0%. The damage morphologies were characterized by a focused ion beam scanning electron microscope (FIB-SEM, Carl Zeiss AURIGA Cross Beam), operating at an accelerated voltage of 1 kV. Atomic force microscopy (AFM, Veeco Dimension 3100) with nanometer horizontal and vertical resolutions was also employed to characterize the morphology of the sample surface after coating.

The LIDT testing result, which is shown in Fig. 1, indicated that the laser damage resistance of the e-beam AR coating is not obviously influenced by the pits fabricated on the substrate. The typical damage morphologies of the AR coatings deposited on the substrate with fs-pits were characterized and are shown in Fig. 2. Under the high fluence of 50 J/cm^2 laser irradiation, the local defects strongly absorb the energy of the incident laser, and some materials are even ejected due to the thermalization of the laser energy. The energy accumulated in the damaged region leaves the plasma ablation region molten under a high temperature. Under a relatively low fluence of 34 J/cm^2, as shown in Fig. 3, delamination still occurs in the overcoat. The crater center that exists in the center area of the damage site penetrated deeply into the substrate, as measured by AFM. The damage sites are not far away (<50 μm) from the fs-pit defects, and their laser fluence can be considered to be the

Table 1. AR Coating Samples Listed by Different Coating Parameters[a]

Sample Name	Deposition	Layer Stack[b]	Substrate Cleaning	Temperature (°C)
EB-1	E-B	$S^{\#}$/2L0.5H1.25L/A	SSC	140
EB-2	E-B	S/2L0.5H1.25L/A	SSC	140
EB-3	E-B	S/L/A	SSC	140
SOL	Sol-Gel	S/L/A	SSC	25
A1	E-B	S/2L0.5H1.25L/A	SSC	200
A2	E-B	S/2L0.5H1.25L/A	HF+SSC	200
B1	E-B	S/2L0.5H1.25L/A	SSC	140
B2	E-B	S/2L0.5H1.25L/A	HF+SSC	140

[a]"E-B" denotes the e-beam deposition; "A" denotes air.
[b]"S" denotes substrate; "$S^{\#}$" denotes substrate with fs-pits; "HF" denotes the HF etching.

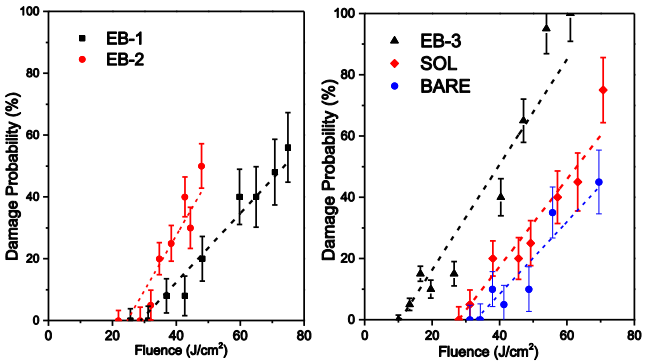

Fig. 1. Damage probability curves of (left) samples EB-1, EB-2; (right) EB-3, SOL, and bare substrate. The dashed lines denote the damage probability fitted curves, which were plotted using the least squares method.

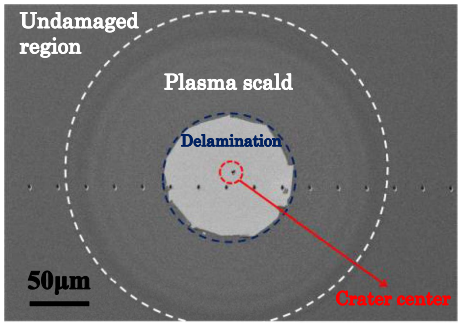

Fig. 2. Typical damage morphologies of the AR coatings with pits on the substrate.

same. For the AR coatings deposited on the substrate without fs-pits, the typical damage morphologies are similar to those coatings with fs-pits. The LIDT results indicate that the damage to the AR coatings may be induced by the "invisible"

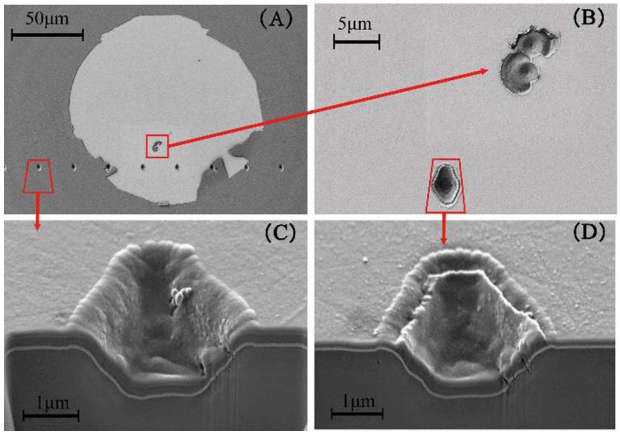

Fig. 3. (a) Damage morphologies on the AR coatings deposited by the e-beam on the fused silica substrate with fs-pits irradiated by a fluence of 34 J/cm^2. Delamination occurred in the plasma scald region under high fluence. (b) The crater center and coated fs-pits after delamination. (c) Cross section of undamaged coated fs-pits. (d) Cross section of damaged fs-pits.

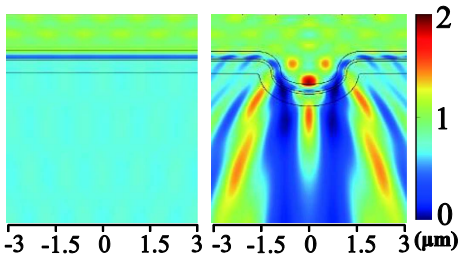

Fig. 4. Simulation of $|E|^2$ field distribution with and without fs-pits with the same color scales for (left) conventional AR coating; (right) pitted AR coating.

nano-scale impurities in the coatings or the interface of the substrate and coating layer. The damage morphologies indicated that the damage is not initiated by the substrate pits, even though the finite element method simulation showed the $|E|^2$ field (the intensity of electric field) was enhanced by ~300% at the substrate and ~35% at the film-substrate interface with a pitted substrate (shown in Fig. 4). The experimental results showed that the effects of the fs-pits are not as significant as we originally predicted. It also showed that the fs-pits on the substrates are not the most influential source of damage. More attention should be paid to the laser damage defects at lower thresholds.

Furthermore, the LIDT of the sol-gel coating, also shown in Fig. 1, is close to that of the bare substrate, which is much

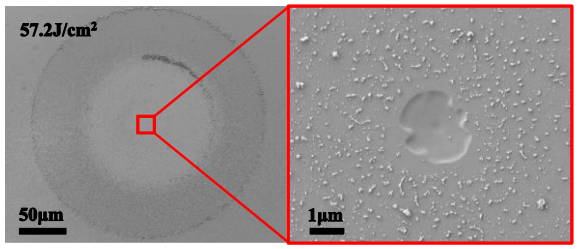

Fig. 5. (Left) Damage morphologies of sol-gel coating irradiated by a laser fluence of 57.2 J/cm^2. (Right) The crater center of the damage site of the sol-gel coating.

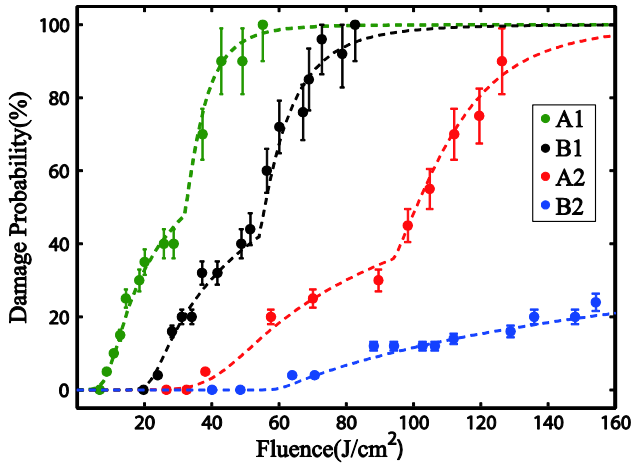

Fig. 6. LIDT of samples A1, A2, B1, and B2. The dots denote the experimental data, and the solid lines denote the fitted curves.

Table 2. Defect Parameters Extracted from the Best-fitted Curves

	d_1 (mm^{-2})	T_1 (J/cm^2)	ΔT_1 (J/cm^2)	d_2 (mm^{-2})	T_2 (J/cm^2)	ΔT_2 (J/cm^2)
A1	18.5	10.2	5.33	200	30.2	9.63
A2	18.7	42.0	15.5	220	95.3	30.0
B1	20.0	22.0	5.25	200	50.9	9.66
B2	8.36	60.8	5.00	—	—	—

higher than that of the e-beam coating. When irradiated by a fluence of 57.2 J/cm^2, the deepest sol-gel coating damage was about 70 nm, and did not reach the substrate, as shown in Fig. 5. The sol-gel coating morphologies in our experiment are similar to those observed previously in [18]. One of the differences between the e-beam and sol-gel deposition methods is the heating process involved. The chemical reactions during the e-beam deposition process are facilitated by a high temperature, and the substrate is often heated for hours in the coating chamber. However, heating processes also negatively impact substrate qualities; particles shift to the surface of substrate and aggregate on the surface because of the thermal motion. The interface coupling effect may be introduced by the change in quality of the fused silica surface.

For the LIDT results of samples A1, A2, B1, and B2, we use the model developed by Krol and co-workers [19] to extract the defect thresholds and densities in the coating layers, which are linked to the shape and slope of the damage probability curves. The ensemble function follows a Gaussian law. The function depends on three parameters: defect density d_i, defect damage threshold mean value T_i, and threshold standard deviation ΔT_i. The damage probability curves under the one-on-one LIDT results are analyzed specifically (Fig. 6). The parameters shown in Table 2 are extracted from the best-fitted curves. Two classes of defects are noted in the samples of A1, A2, and B1 ($i = 1$ and $i = 2$), while sample B2 only manifested one kind of defect ($i = 1$). For single nanosecond-order pulse irradiations, low-threshold defects ($i = 1$) are the key factors leading to laser-induced coating damage. For samples A1 and A2, which share the same coating temperature of 200 °C, the best-fitted curve has the parameters of $d_1(A1) \approx d_1(A2)$, $d_2(A1) \approx d_2(A2)$ and $T_1(A1) < T_1(A2)$, $T_2(A1) < T_2(A2)$, and the threshold deviation of $\Delta T_1(A1) < \Delta T_1(A2)$, $\Delta T_2(A1) < \Delta T_2(A2)$, where the threshold results, in particular, show that different substrate surface qualities can indeed affect the LIDT of the coating. Samples A1 and B1, with same quality of substrate but prepared at different coating temperatures, had nearly the same threshold deviations, but the threshold of B1 was two times higher than that of sample A1, which indicates that the low coating temperature can reduce the shift of absorption defect on the interface of the substrate and coating layer [8,9]. In our experiment, the intensity of the interface coupling effects can be simply estimated by the low-threshold defects density (d_1) and low-threshold defects damage threshold (T_1). The intensity of the interface couple effect would be weaker with a higher T_1 and a lower d_1.

In conclusion, a three-step systematic approach was employed to understand the interface coupling effects of the substrate surface and coatings on the laser resistance of 1 ω, 1064 nm coatings in our experiments. First, the impurities in the subsurface play a more important role than any structural surface defects in the laser-induced damage of the AR coating. Second, the comparison of the e-beam and sol-gel deposition technologies indicated that the heating process might be a key factor in coupling effects. Substrate subsurface impurities may be shifted to the surface during the heating process, and the impurities are then aggregated and reconstituted at the surface by thermal motion. Third, the intensity of the interface couple effect of the e-beam coating can be reduced by using a lower deposition temperature and better substrate surface quality (for example, HF etching before coating). This mitigation of the interface coupling effect could help researchers improve the LIDT of optical film coatings.

Funding. National Natural Science Foundation of China (NSFC) (F050602); International Science & Technology Cooperation Programs (2012DFG51590).

REFERENCES

1. D. Hu, J. Dong, D. Xu, X. Huang, W. Zhou, X. Tian, D. Zhou, H. Guo, W. Zhong, X. Deng, Q. Zhu, and W. Zheng, Chin. Opt. Lett. **13**, 041406 (2015).
2. S. R. Qiu, J. E. Wolfe, A. Monterrosa, W. A. Steele, N. E. Teslich, M. D. Feit, T. V. Pistor, and C. J. Stolz, Proc. SPIE **7842**, 78421X (2010).
3. Y. Chai, M. Zhu, Z. Bai, K. Yi, H. Wang, Y. Cui, and J. Shao, Opt. Lett. **40**, 1330 (2015).
4. Z. Yu, H. He, W. Sun, H. Qi, M. Yang, Q. Xiao, and M. Zhu, Opt. Lett. **38**, 4308 (2013).
5. W. Liu, C. Wei, K. Yi, and J. Shao, Chin. Opt. Lett. **13**, 041407 (2015).
6. D. W. Camp, M. R. Kozlowski, L. M. Sheehan, M. A. Nichols, M. Dovik, R. G. Raether, and I. M. Thomas, Proc. SPIE **3244**, 356 (1998).
7. C. J. Stolz, Proc. SPIE **7842**, 784206 (2010).
8. J. Yang, K. Yi, C. Wei, G. Hu, H. Cui, and J. Shao, High Power Laser Part. Beams **26**, 072011 (2014).
9. J. Yang, K. Yi, M. Yang, G. Hu, and J. Shao, Proc. SPIE **9238**, 92380F (2014).
10. T. I. Suratwala, L. L. Wong, P. E. Miller, M. D. Feit, J. A. Menapace, R. A. Steele, P. A. Davis, and D. Walmer, J. Non-Cryst. Solids **352**, 5601 (2006).
11. J. Neauport, L. Lamaignere, H. Bercegol, F. Pilon, and J. C. Birolleau, Opt. Express **13**, 10163 (2005).
12. J. Yoshiyama, F. Y. Genin, A. Salleo, I. Thomas, M. R. Kozlowski, L. M. Sheehan, I. D. Hutcheon, and D. W. Camp, Proc. SPIE **2744**, 220 (1997).
13. Y. Chai, M. Zhu, K. Yi, H. Qi, H. Wang, W. Sun, Z. Yu, Z. Bai, Y. Zhao, and J. Shao, Proc. SPIE **9237**, 92370 (2014).
14. Z. Yu, H. He, X. Li, H. Qi, and W. Liu, Chin. Opt. Lett. **11**, 073101 (2013).
15. W. Liu, C. Wei, J. Wu, Z. Yu, H. Cui, K. Yi, and J. Shao, Opt. Express **21**, 22476 (2013).
16. J. Liu, W. Zhang, H. Cui, J. Sun, H. Li, K. Yi, and M. Zhu, Chin. Opt. Lett. **12**, 083101 (2014).
17. S. Kimura and C. Munakata, Appl. Opt. **27**, 84 (1988).
18. G. Hu, Y. Zhao, J. Shao, K. Yi, D. Li, X. Liu, and Q. Xiao, J. Opt. Soc. Am. B **30**, 1186 (2013).
19. H. Krol, L. Gallais, C. Grezes-Besset, J. Y. Natoli, and M. Commandre, Opt. Commun. **256**, 184 (2005).